Title: Centrifuge modelling of suction anchors under multidirectional loading for shared mooring applications

Author 1

- Cristian Yair Soriano Camelo, postdoctoral researcher*
- Geotechnical Centrifuge Laboratory (GERS-CG), Université Gustave Eiffel, Nantes, France
- https://orcid.org/0000-0001-9530-0185

Author 2

- Matthieu Blanc, GERS-CG laboratory director
- Geotechnical Centrifuge Laboratory (GERS-CG), Université Gustave Eiffel, Nantes, France
- https://orcid.org/0000-0003-0603-487X

Author 3

- Benjamin Cerfontaine, Associate Professor
- Infrastructure Group, University of Southampton, Southampton, United Kingdom
- https://orcid.org/0000-0002-4833-9412
- Author 4
- Luc Thorel, director of research
- Geotechnical Centrifuge Laboratory (GERS-CG), Université Gustave Eiffel, Nantes, France
- https://orcid.org/0000-0002-0218-4144

Full contact details of the corresponding author.
***cristian.soriano-camelo@univ-eiffel.fr**

- Number of words in the main text **4559** (excluding abstract and references), number of tables **2** and number of figures **19**

Abstract (150 – 200 words)

Shared anchors for floating offshore wind turbines (FOWTs) offer potential cost savings, but their geotechnical performance under complex multidirectional mooring loads in soft clay requires better understanding. To address this, centrifuge modelling was conducted at 75-g on model suction anchors in normally consolidated kaolin clay. The experiments simulated several loading scenarios, including monotonic pull-out and multidirectional loading patterns representing shared anchor configurations (three lines at 45° inclination to the horizontal plane, spaced by 120° azimuthally). Three load tests were performed: a monotonic reference test and two multidirectional tests involving alternating and simultaneous line loading. Measurements included the anchor load-displacement response and excess pore pressures with complementary data from digital image correlation. The baseline monotonic test yielded an ultimate capacity of approximately 4 MN. Alternating line loading induced progressive downward displacements, while simultaneous two-line loading produced a trend of upward movement. Simultaneous loading also led to greater horizontal displacements, reflecting increased mobilisation under compound loading paths. Post-multidirectional monotonic tests revealed reductions in anchor capacity between 10% and 38%, depending on the load path history and inclination. This work delivers benchmark data clarifying suction anchor behaviour under multidirectional loads, to validate numerical models and optimize shared anchor designs for FOWTs.

Keywords

Offshore renewable energy; Centrifuge modelling; Geotechnical engineering

List of notations

σ'_v is the vertical effective stress

γ' is the effective unit weight of the soil

D is the diameter of the anchor

L is the length of the anchor

T is the anchor wall thickness

W is the weight of the anchor

F is the load applied to the anchor

$F_{ult,1}$ is the baseline capacity of anchor 1

$F/F_{ult,1}$ is the normalised load with respect to baseline capacity

s_u is the undrained shear strength of the clay

N_t is the t-bar factor for undrained shear strength calculation

N is the centrifuge scale factor

g is the earth's gravity acceleration

t is the time recorded during the centrifuge tests

d is the displacement of the anchor

β is the inclination angle of the load applied at the anchor padeye

θ is the anchor rotation angle

H_{ult} is the estimated horizontal load capacity of the anchor at the optimal depth

V_{ult} is the estimated ultimate vertical load capacity of the anchor

ΔPwP is the change in excess pore pressure

Introduction

The deployment of offshore wind energy infrastructure is expanding to meet renewable energy targets, requiring installations in deeper waters (>60 m), where floating offshore wind turbines (FOWTs) are necessary (Goupee et al., 2014). These turbines rely on effective mooring systems anchored to the seabed to maintain stability under environmental forces (Jiang, 2025). Suction caissons, constitute an anchoring solution for FOWTs, due to their relative installation efficiency, silent installation, high holding capacity against combined loads arriving from floating structures and versatility for installation in clay and sand seabeds (Cerfontaine et al.,2023; Coughlan et al., 2025). Mooring systems contribute significantly to capital costs, accounting for approximately 10% to 15% of total project expenses (James and Ros, 2015), driving efforts towards cost optimization.

To reduce costs and minimise the seabed footprint, the concept of 'shared anchors' or 'multiline anchors'- where a single anchor secures mooring lines from multiple FOWTs- is gaining attention (Xu et al., 2024, Devin et al., 2021). Shared anchors decrease the number of required foundations, reducing material use, installation time, vessel mobilization, and site investigations (Lee and Aubeny, 2023; Fontana et al., 2018; Diaz et al., 2016). The operational feasibility of this concept has been demonstrated in projects such as Hywind Tampen, where 19 suction anchors were installed for an 11-FOWT farm (Ore Catapult and Arup, 2024; Sloan et al., 2022). Furthermore, numerical simulations indicate that compared with single-turbine mooring configurations, shared anchors can effectively mitigate peak horizontal loads, potentially achieving reductions of up to 50% (Pillai et al., 2022; Fontana et al., 2018).

Despite increasing interest in shared anchors and their potential benefits, their geotechnical behaviour under complex, multi-directional loading from multiple mooring lines remains insufficiently understood. In particular, it is unclear whether anchor capacity increases, decreases, or remains unchanged following cyclic loading. Anchor capacity is influenced by the loading rate relative to the rate of pore pressure dissipation, which affects the mobilised shear strength. Moreover, loading history can progressively alter the stress state and density of the surrounding soil, further affecting the available strength. These processes can lead to capacity changes—either reductions or gains—relative to the initial monotonic capacity, often by factors ranging from 2--5 (Cerfontaine et al., 2023).

Some studies have reported capacity degradation due to cyclic loading. For example, Chen and Randolph (2007) used centrifuge tests to investigate the uplift capacity of suction anchors in normally consolidated clay under sustained and cyclic loading. They applied load packages comprising 50 cycles with amplitudes between 50% and 90% of the monotonic capacity, over prototype times ranging from 17--34 days, and observed a reduction in the holding capacity to 72%--86% of the undrained monotonic capacity. Similarly, field tests by Dyvik et al. (1993) revealed that the bearing capacity of suction anchors in clay under cyclic loading decreased to approximately 66%--82% of the static capacity. Conversely, other studies have reportes capacity enhancement following cyclic loading. Lee et al. (2024) conducted centrifuge experiments on suction anchors in soft clay under cyclic inclined pull-out loading and reported a 32% increase in postcyclic monotonic capacity. This gain was observed when the monotonic load was applied immediately after the cyclic loading phase, indicating that reconsolidation was not required for the strength increase. The concept of "whole-life changes" in capacity, as outlined by Gourvenec (2020), emphasizes that cyclic loading, when combined with consolidation, can increase the strength of soft clays. These changes in soil properties may result in increased anchor capacity—an effect that is often overlooked in conventional design approaches.

A knowledge gap remains regarding the response of suction anchors embedded in soft, normally consolidated clay under simultaneous loads from multiple mooring lines, which are representative of shared anchor configurations. This study aims to address this gap by developing and testing an experimental setup within the geotechnical centrifuge at Université Gustave Eiffel, specifically designed to apply controlled, multidirectional loading to suction anchors. The configuration allows up to three inclined loads to be applied simultaneously to a single suction anchor, with mooring lines spaced 120° azimuthally and pulling at 45° to the horizontal plane. To evaluate the setup's performance and reliability, three simplified monotonic load/unload paths were applied. The anchor response was monitored via load cells on each mooring line to measure the applied forces and determine the mobilised capacity. Overall anchor displacements were recorded via laser displacement transducers. Additionally, pore pressure transducers were embedded at the top and base of the anchors to measure the evolution of excess pore pressures—particularly suction—during loading. The experimental results provide benchmark data for validating numerical models and offer initial insights into anchor behaviour under

controlled multi-directional loading, forming the basis for future, more complex experimental campaigns.

2. Experimental setup and model preparation

2.1 Description of the centrifuge tests

A series of loading tests was conducted on three suction anchors installed in normally consolidated clay. The experiments utilized the 4.5-m-radius geotechnical centrifuge at the Université Gustave Eiffel, Nantes campus (formerly LCPC and IFSTTAR) (Corte, 1984).

2.2. Sample preparation

Speswhite kaolin, which is a well-documented material extensively employed in centrifuge modelling (Springman, 1993; Raines and Garnier, 2004; Thorel et al., 2011; Lau, 2015), was used to build a normally consolidated clay profile. The clay sample was prepared by mixing kaolin with water to achieve a water content of 90% before consolidation. The resulting slurry was then poured into a cylindrical container (895 mm in diameter and 700 mm high), on a 90 mm thick base drainage layer placed at the bottom of the container to facilitate consolidation of the clay. A total amount of approximately 280 kg of kaolin clay was required to prepare the clay sample.

The clay profile was constructed in four layers, each subjected to a specific preconsolidation pressure determined from a target effective vertical stress profile (assuming an effective unit weight, $\gamma' = 6$ kN/m³). Consolidation was performed at 1-g using a computer-controlled hydraulic press over a total period of one month, similarly to Khemakhem (2012). Figure 1 illustrates the target consolidation pressures for each sublayer and the resulting thickness of the clay profile upon completion of consolidation.

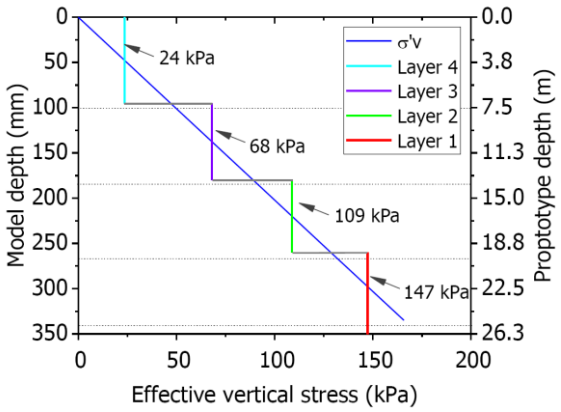

Figure 1. Target pre-consolidation pressures to build a normally consolidated clay profile (right axis in prototype scale)

2.3 Experimental setup

A prototype suction anchor with a diameter (D) of 4.5 m and a length (L) of 15.0 m, resulting in a length-to-diameter ratio (L/D) of 3.3, was selected to be comparable to the Hywind Tampen wind farm, where the shared anchor concept has been implemented (Coughlan et al., 2025). A centrifuge scaling factor of N=75 was adopted to enable the testing of three model suction anchors in one consolidated sample. Each anchor included three padeyes, positioned at approximately two-thirds of the anchor length from the top, to enable inclined load application from three mooring lines. Figure 2 presents a plan view of the anchor layout and a representation of the mooring line load application points (L1, L2, and L3). The center-to-center spacing between adjacent anchors is approximately 6.4D, and the distance from each anchor center to the model container boundary is approximately 3.6D. Table 1 summarizes the model and prototype dimensions. An overview of centrifuge scaling laws used in the tests is provided by Garnier et al. (2007).

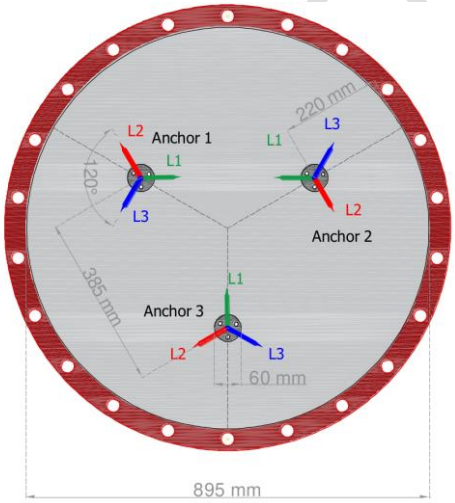

Figure 2. Plan view of the experimental setup: location of the suction anchors

Table 1. Prototype and model dimensions

	Dimension	Model (1/75)	Prototype
Suction Anchor	Material	Aluminum	
	D,diameter	60.0 mm	4.5 m
	L, length	200.0 mm	15.0 m
	L/D	3.3	3.3
	t (wall thickness)	0.4 mm	3.0 cm
	D/t	150.00	150
	W, weight	330.0 g	1.39 MN
	W', buoyant weight	277.2.0 g	1.14 MN
Model Container	Height	700 mm	52.5 m
	Diameter	895 mm	67.1 m
	Water table	50 mm	3.75 m
Clay sample	Thickness	350 mm	26.3 m

Figure 3 shows the experimental setup used in the centrifuge test. The setup included a combination of fixed components (parts No.1 to No. 7 in Figure 3b) designed to support the actuators, pulleys, cameras, and laser sensors, along with movable components such as the mooring lines and anchors. Three electric actuators (Figure 3a) were employed to apply the loads and were instrumented with load cells (TME cells with 5 kN capacity). An extension piece was attached to the top of the anchor (part No. 8), comprising an aluminium pipe and a circular cap fabricated using a 3D printer. This extension was designed to facilitate additional measurements of the anchor's rotations, vertical displacements, and translational movements. Although lightweight, the extension added a surcharge equivalent to 10% of the anchor's total weight.

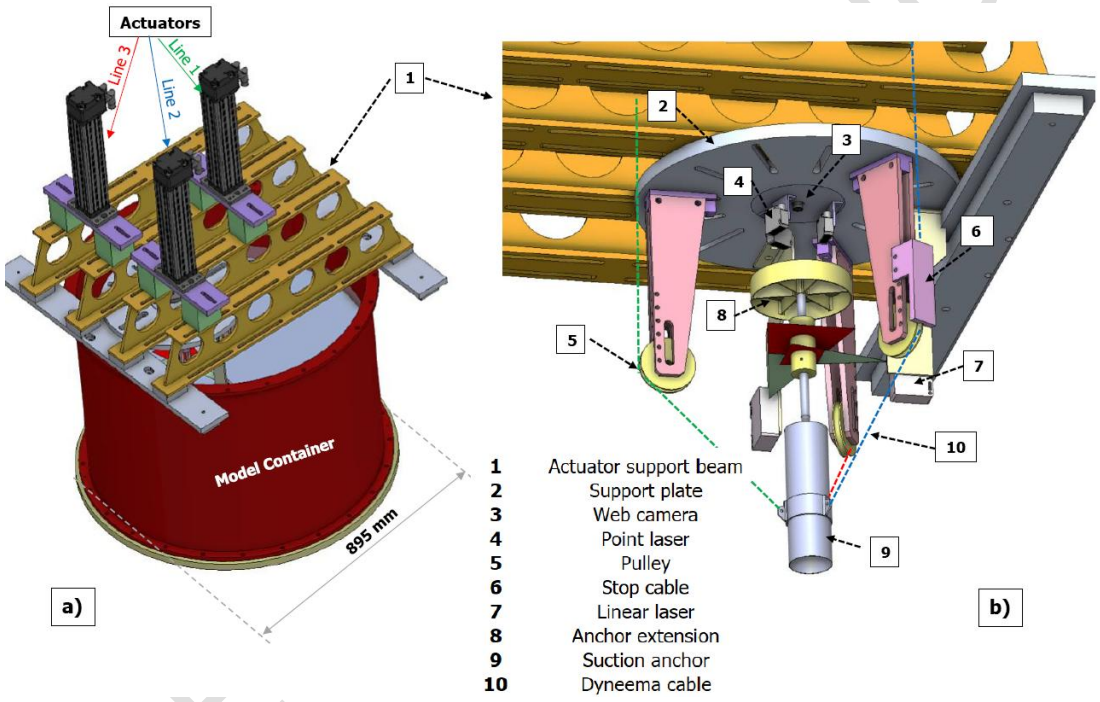

Figure 3. Experimental setup for multiline anchor testing. a) Perspective view of the model container and actuators. b) Detailed view of an anchor and instrumentation.

A rotating assembly was developed to reduce the time between tests, by allowing the anchor testing location within the model container to be repositioned through rotation, while the container itself remained stationary. The data logging system (Quantum HBK multi IO) was integrated directly into this rotating assembly, which minimized the need for repeated disconnection and reconnection of sensor cables during the testing sequence. Figure 4 shows the position of the rotating assembly during the tests on anchor 1 and anchor 3 (Figure 2).

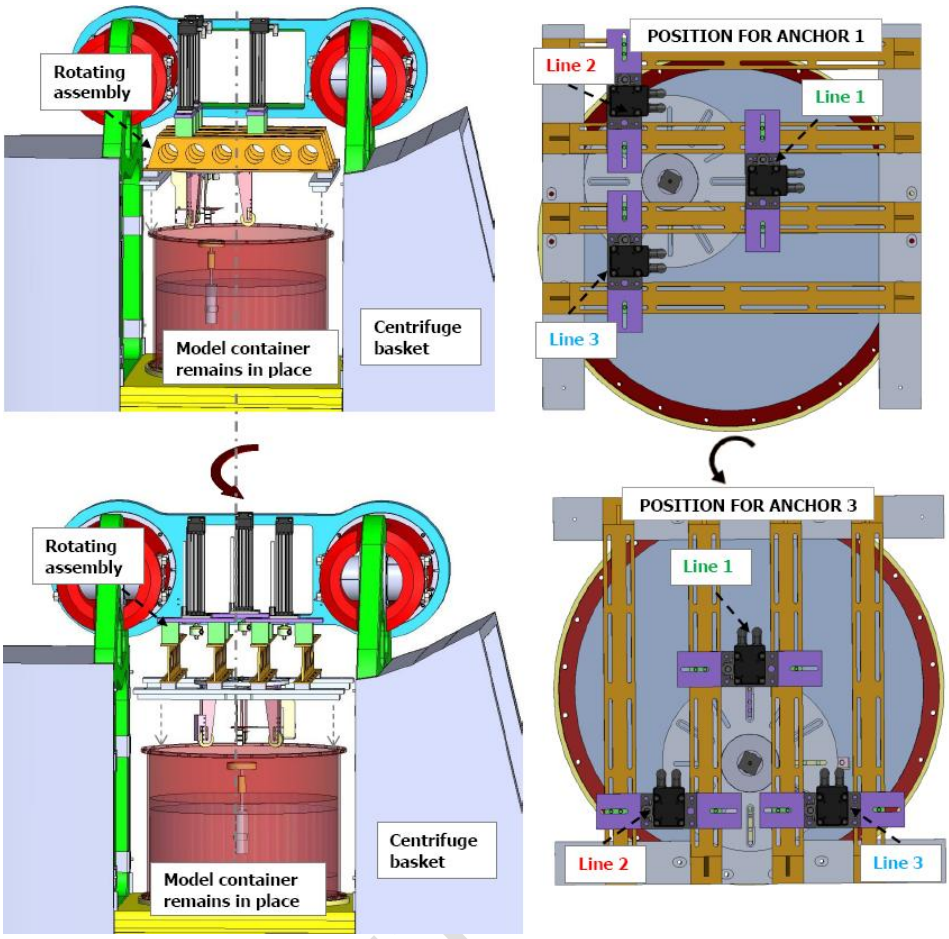

Figure 4. Rotating assembly to test various anchor locations

2.4 Suction anchor installation

The anchors were installed at 1-g by manually pushing them into the clay. While suction is used for offshore anchor installation, jacking or manual pushing at 1g is a suitable alternative in centrifuge modelling. Chen and Randolph (2007) reported no significant differences in axial capacity or radial stress changes between caissons installed by suction in-flight and those jacked at 1-g in normally consolidated clay. The installation depth corresponded to the full length of the anchors (200 mm). During this process, the top valves of the anchors were kept open to allow trapped air within the caisson to escape, as illustrated in Figure 5a and Figure 5c. To ensure vertical alignment during insertion, a guide constructed from an aluminium pipe was utilized; this guide could later be removed by unscrewing it from the anchor's top cap. The guide mechanism also incorporated a 3D-printed support piece (Figure 5b), which was attached to the main top plate (part No. 2 in Figure 3) to guarantee the verticality of the anchor during installation.

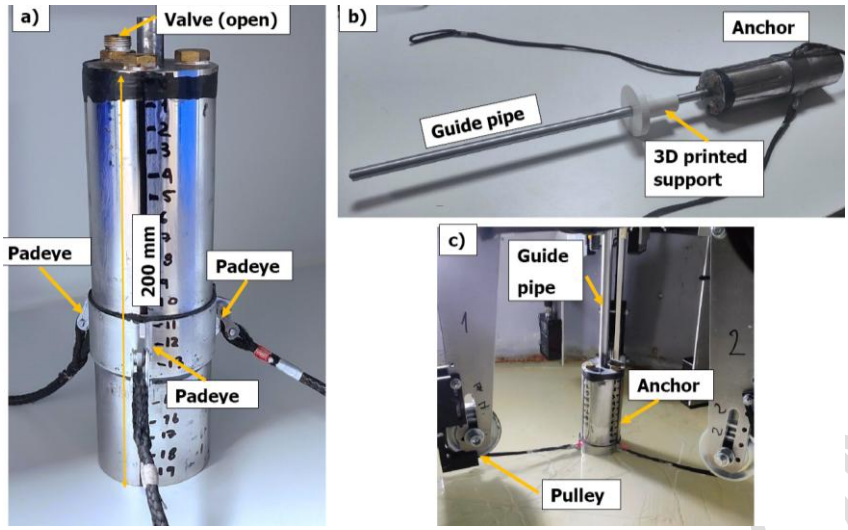

Figure 5. a) Detail of a model anchor; b) guide mechanism for installation; c) anchor installation at 1-g

During anchor installation, the mooring lines were manually pretensioned simultaneously to cut through the surrounding clay and ensure a consistent starting point for load application. This process established a uniform exit point at the clay surface for all three lines. Once this was achieved, the pretension was released. Figure 6 shows an anchor after 1g installation, including the footprint left by the mooring lines during pretensioning. To ensure correct alignment of the lines within the pulleys, 3D-printed components, referred to as stop cables, were used (part No. 6 in Figure 2). The mooring lines were made of 4 mm diameter SK78 Dyneema synthetic ropes. These cables have a Young's modulus ranging from 108 GPa to 113 GPa (Vlasblom, 2018), a linear weight of approximately 9 g/m, and a load resistance of 1300 daN at 1% elongation (LIROS, 2025).

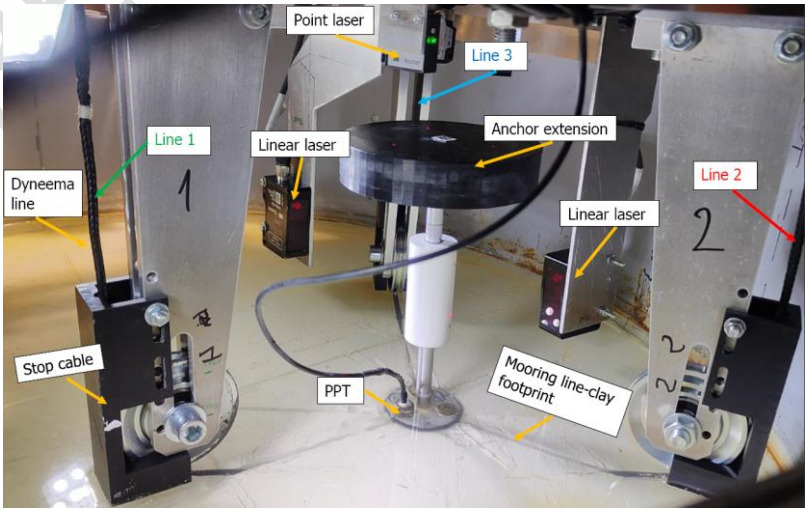

Figure 6. A view of a model anchor and instrumentation after installation at 1-g

2.5 Model Instrumentation

The centrifuge model was instrumented as follows. Druck pore-pressure transducers (PPTs) were embedded during clay consolidation at three elevations: (i) one anchor diameter (1D) below the caisson base, (ii) at the caisson base, and (iii) at the caisson top (Figure 7a). The clay surface settlements were measured with LVDTs. Lateral displacements of the anchors were tracked using linear laser transducers (Baumer OM20), configured to detect the centre of cylindrical objects within their measurement field. By arranging two linear lasers perpendicularly, the movement of the anchor extension could be tracked in a x–y (horizontal) plane (Figure 7b). Additional Baumer OM20 point lasers were positioned above the model to measure vertical displacements at the top of the extension piece and estimate anchor rotations on the basis of their relative distance (Figure 7c).

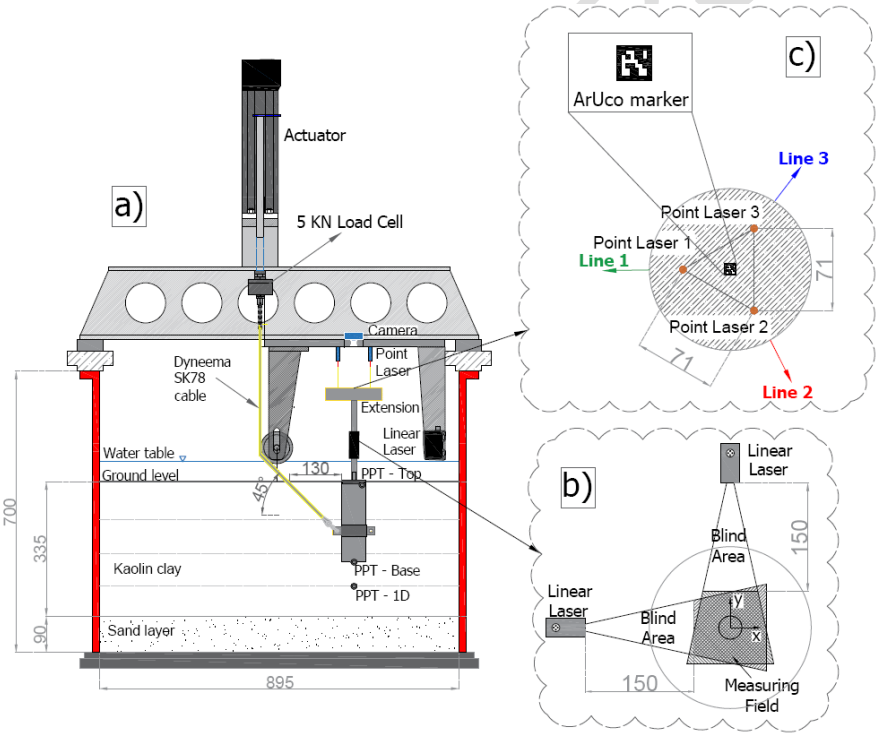

Figure 7. Model instrumentation. a) Lateral view or an anchor and connection of one mooring line. b) Linear lasers position to track lateral displacements. c) Point lasers to track vertical displacements and detail of an ArUco marker

To obtain additional displacement data via digital image correlation (DIC), an ArUco marker (Garrido et al., 2014) was placed on the upper extension of the anchor (Figure 7c). A camera (IP network camera HDI-47) mounted above the anchors enabled tracking of the marker's

displacement, primarily within a planar projection. The tracking process was conducted using Blender software, and the detailed procedure for performing these analyses was outlined by Soriano et al. (2021).

2.6. Centrifuge Testing Programme

Three load tests were conducted: a monotonic test to establish the baseline anchor capacity, followed by two multidirectional loading tests. The primary objective was to evaluate the performance of the experimental setup using simplified load paths. Although these load paths do not replicate specific offshore conditions, they serve as a proof of concept to demonstrate the setup's ability to apply and monitor controlled multiline loading. This framework can later be extended to incorporate cyclic and time-dependent loading scenarios. While the current tests do not aim to fully characterise anchor behaviour, the results offer initial insights that may support the calibration of numerical models and guide the design of future studies under more realistic loading conditions. The testing conditions of the anchors are summarized in Table 2.

Table 2. Identification of loading tests for the suction anchors

Anchor	Load condition	Load rate (model scale)
1	Monotonic	30 mm/min
2	Multidirectional alternated	30 mm/min
3	Multidirectional two lines alternated	30 mm/min

The loading sequence varied for each anchor but maintained a consistent load inclination of 45° to the horizontal. Anchor 1 was subjected to a monotonic inclined load applied by mooring line L1 (Figure 3). This test established a baseline for the anchor capacity. Anchor 2 underwent a series of monotonic loads applied alternately through lines L1, L2, and L3, each inclined at 45°. The load amplitude progressively increased in successive cycles, as illustrated in Figure 8a. This alternating sequence resulted in varying load components, which can be decomposed into three orthogonal directions: x and y in the horizontal plane, and z in the vertical plane. Figure 8b shows the evolution of these load components during a representative load cycle. For reference, the x-axis was defined as the positive direction of the load applied to Line L1

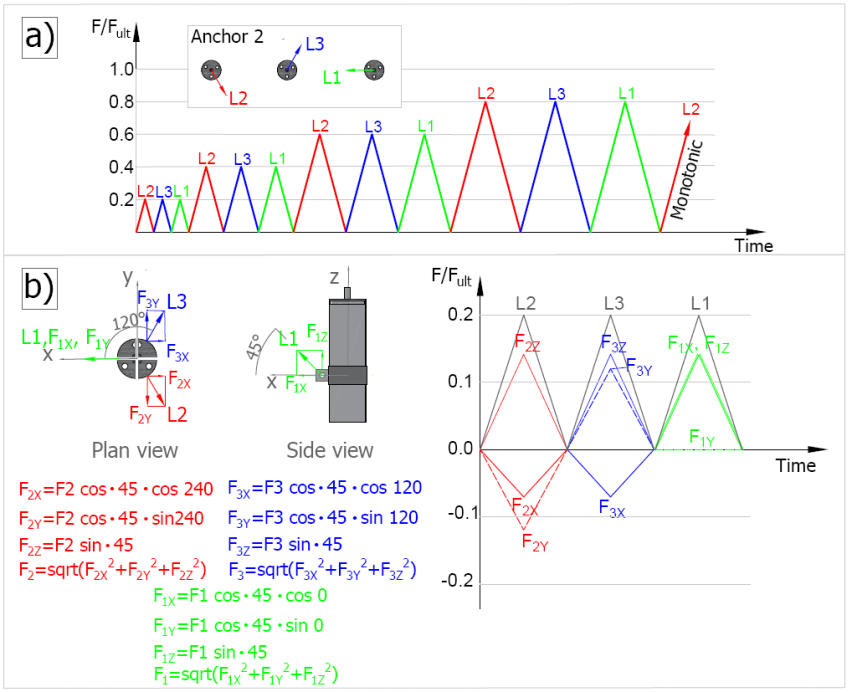

Figure 8. Anchor 2: progressively increasing amplitude monotonic loads applied by alternating mooring lines

Anchor 3 was tested under simultaneous loading from two mooring lines at a time, also inclined at 45°, alternating between line pairs (L1–L2, L2–L3, L1–L3). The load amplitude progressively increased in each pairwise sequence, as depicted in Figure 9a. The superposition of two inclined loads resulted in a resultant force with a steeper inclination than the individual line loads. Figure 9b provides a schematic representation of this combined loading and the calculation of the resultant force from a pair of forces.

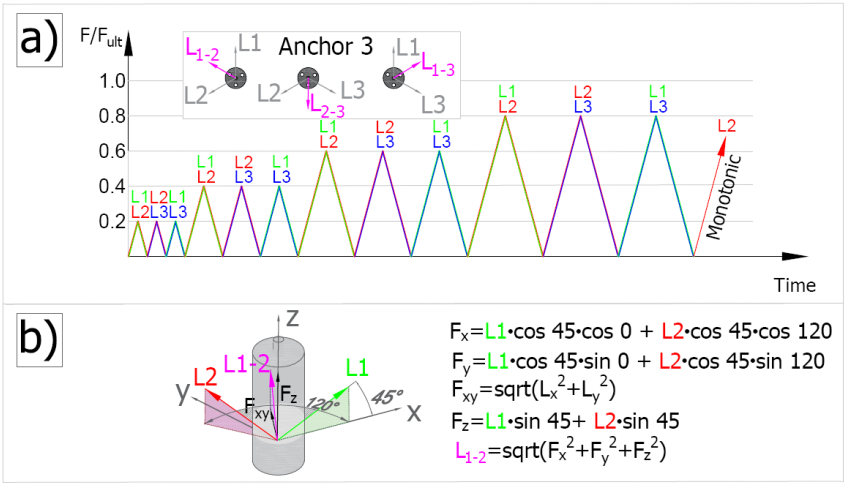

Figure 9. Anchor 3: progressively increasing amplitude monotonic loads applied by two mooring lines simultaneously.

Note that Figure 8 and Figure 9 present the load sequences schematically, without detailing the time intervals between load steps, for clarity.

2.7 Test procedure

Anchor testing was carried out over three days, with one test conducted per day. The swing up of the model consisted of increments of 10-g until reaching the target acceleration level for the test (75-g). Once at the target acceleration, the model was kept in flight for 5 hours. To evaluate the in-situ soil strength conditions prior to each anchor test, a T-bar penetration test was performed in-flight each day. These tests were conducted at a penetration rate of 2 mm/s using a T-bar penetrometer with a diameter of 5 mm and a length of 20 mm, resulting in a projected area of 100 mm².

The undrained shear strength profiles shown in Figure 10 were derived from data recorded by a potentiometer attached to the T-bar actuator and force measurements from a load cell positioned at the top of the T-bar. A T-bat factor N_t=10.5 was used in the calculations (Stewart and Randolph, 1991). Only two profiles are shown due to sensor malfunction during the first test. Additionally, after the centrifuge was stopped, hand shear vane tests were conducted at various depths via a Pilcon vane tester with a 33 mm diameter and 50 mm blade length. This method, which is commonly used in clay-based centrifuge studies (Divall et al., 2016; Panchal et al., 2020), provides additional undrained strength data. The results from both methods indicate that the strength profile increases with depth, from approximately 2.5 kPa at the surface to 10 kPa at the anchor tip depth of 15 m. The close agreement between the vane and T-bar measurements confirms their complementarity in characterizing the clay profile. A data sampling frequency of 10 Hz was used for monitoring the consolidation phase, whereas a higher frequency of 100 Hz was employed during the anchor load tests and the T-bar tests.

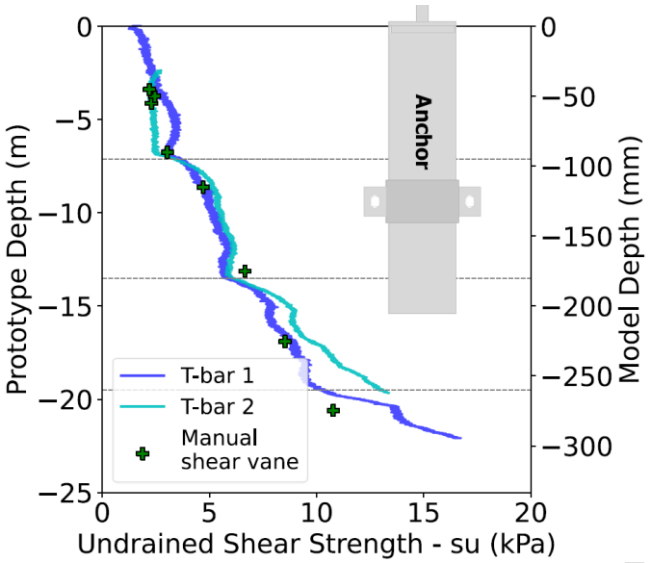

Figure 10. Undrained shear strength profiles measured in-flight and 1-g shear hand vane tests

3. Test results

3.1 Monotonic load test – Anchor 1

The normalized load–displacement response of Anchor 1 is shown in Figure 11a. The load was measured using the actuator load cell, and the displacements corresponded to those imposed by the actuator. The load increased until it reached a plateau at $F_{1,ult}$ = 4 MN, which was defined as the baseline capacity for subsequent multidirectional tests. Displacements were normalized by the anchor diameter D. To approximate the displacement at the loading depth (labelled d_{xz} in Figure 11a), a combination of laser measurements was used. One linear laser measured the lateral displacement (d_1), while point lasers were used to estimate the anchor's rotation (θ). The vertical displacement was estimated as the average of the vertical displacements recorded by the point lasers positioned at the top of the anchor extension (d_z). This combined approach allowed the construction of an approximate load–displacement curve at the load application depth. However, the accuracy was limited by the measurement range of the lasers. An offset was applied to this load-displacement curve to align its trend with the actuator-derived curve at approximately 0.2D normalized displacement. The difference between the actuator-imposed displacement and the response at the anchor load depth indicates that some initial actuator movement is required before effective load transfer to the anchor occurs. This may reflect slack in the system or interactions between the mooring line and surrounding clay that must be overcome before the anchor resists the load.

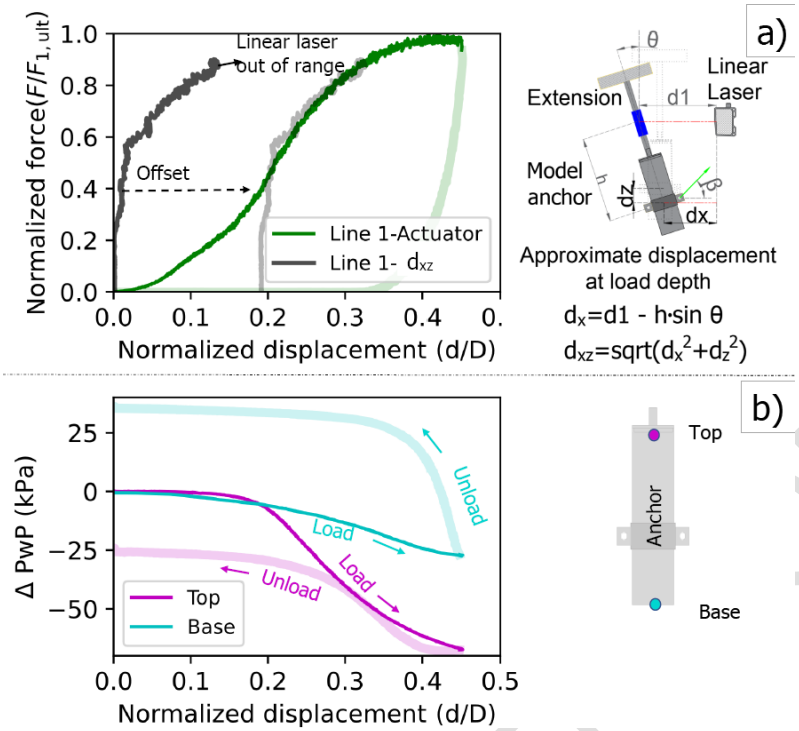

Figure 11. Anchor 1: load-displacement response and excess pore pressure measurements at the top and at the base of the anchor

To facilitate a comparison of pore pressure responses, an initial offset was applied to the measured values, setting them to zero at the start of loading (ΔPwP in Figure 11b). During loading, both pore pressure transducers (PPTs) recorded decreasing values beginning near a normalized displacement of 0.2D, indicating load transfer to the anchor. The development of these negative excess pore pressures indicates the progressive mobilisation of reverse end bearing capacity and confirms the effective sealing of the anchor's top cap.

After unloading, residual negative pore pressure remained inside the anchor. Conversely, at the base, the excess pore pressure became positive, likely because of anchor settlement during unloading, resulting in pressure build-up in the underlying soil.

3.2. Multidirectional alternated load test – Anchor 2

The force–displacement responses for each mooring line connected to Anchor 2 are shown in Figure 12. The loading sequence begins with Line 2, followed by Line 3, and concludes with Line 1. All forces are normalized by the monotonic capacity of Anchor 1 ($F_{1,ult}$ = 4 MN), and the displacements correspond to actuator-imposed values. While anchor displacements were also monitored, they are not shown here due to limitations in capturing full 3D movements and

the potential for laser sensor range exceedance at large displacements. Normalised actuator displacements are therefore used consistently across tests to enable comparison. Line 2, which was also the first to be loaded, was subjected to an additional cycle at the end of the sequence (Cycle 5), during which a monotonic load was applied until a plateau was reached at approximately 3.6 MN (0.9 $F/F_{1,ult}$). For reference, the load–displacement curve from the monotonic test on Anchor 1 is included in the figure. Across the load–unload cycles, a two-phase trend is observed: an initial concave slope up to a normalized displacement of approximately 0.2*D*, followed by a change in stiffness. This transition is consistent with the behaviour noted in Anchor 1, where effective load transfer to the anchor appears to begin beyond this displacement threshold. Overall, the curves follow a backbone response pattern when compared with the monotonic loading of Anchor 1.

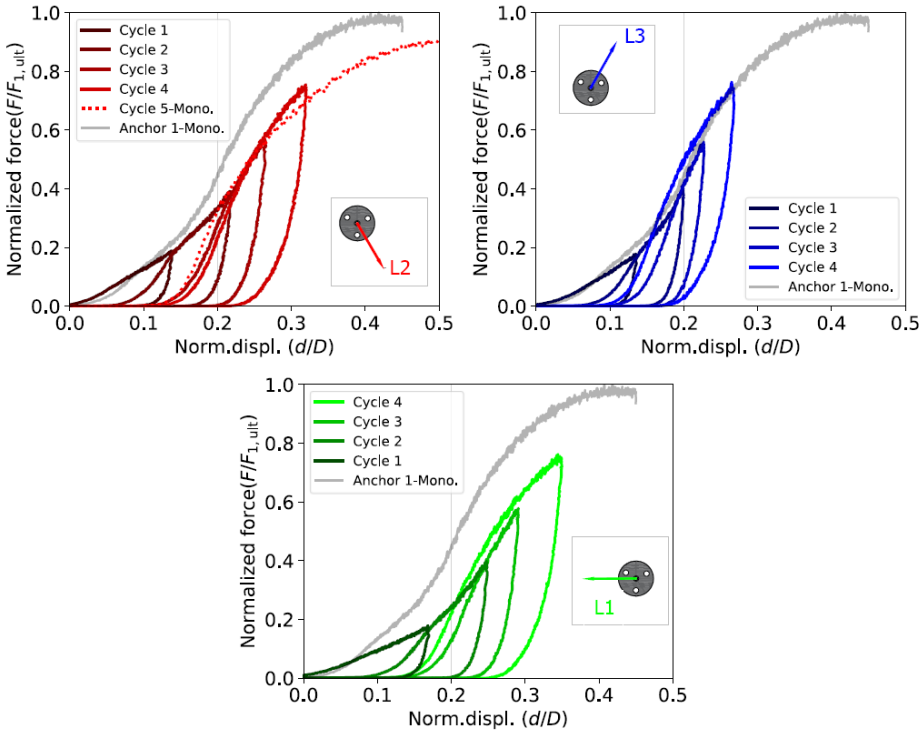

Figure 12. Anchor 2: Load displacement curves for each mooring line

Figure 13 shows the average vertical displacements of the anchor, measured by the lasers positioned at the top of the extension piece (Figure 7c), along with the applied actuator loads. During Cycle 1, no significant pullout displacement was observed, indicating that part of the applied load was mobilized before reaching the anchor, which is consistent with previous observations. From Cycle 2 onwards, progressive settlement of the anchor was recorded, with

increased displacements occurring primarily during the unloading phases. Overall, the amplitude of the vertical displacement loops correlates with the magnitude of the applied loads.

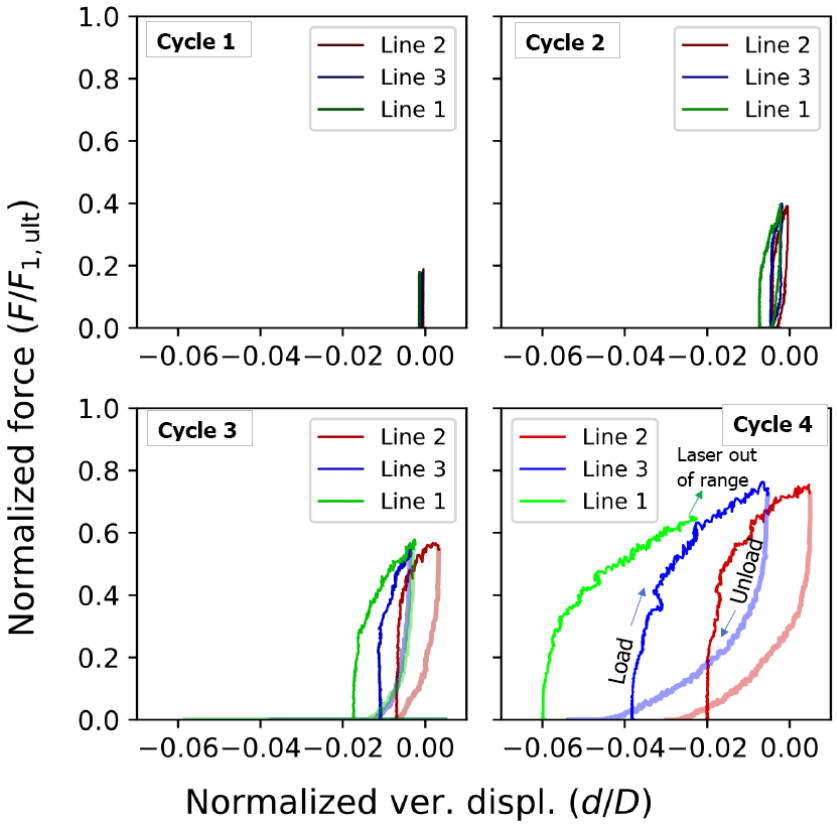

Figure 13. Anchor 2: Relationship between applied load and average vertical displacements

Figure 14a presents the time history of the loads applied to the anchor, demonstrating the consistent performance of the force control system throughout the test. Figure 14b shows the excess pore pressure measurements recorded at the top and base of the anchor. Both transducers exhibit similar trends during loading, with negative excess pore pressures (suction) developing in proportion to the applied load magnitude. The transducer at the base also shows a gradual increase in pore pressure over the test sequence, indicating a net buildup of positive pressure. This trend is attributed to the cumulative downwards movement (settlement) of the anchor under repeated load–unload cycles, as illustrated in Figure 14c.

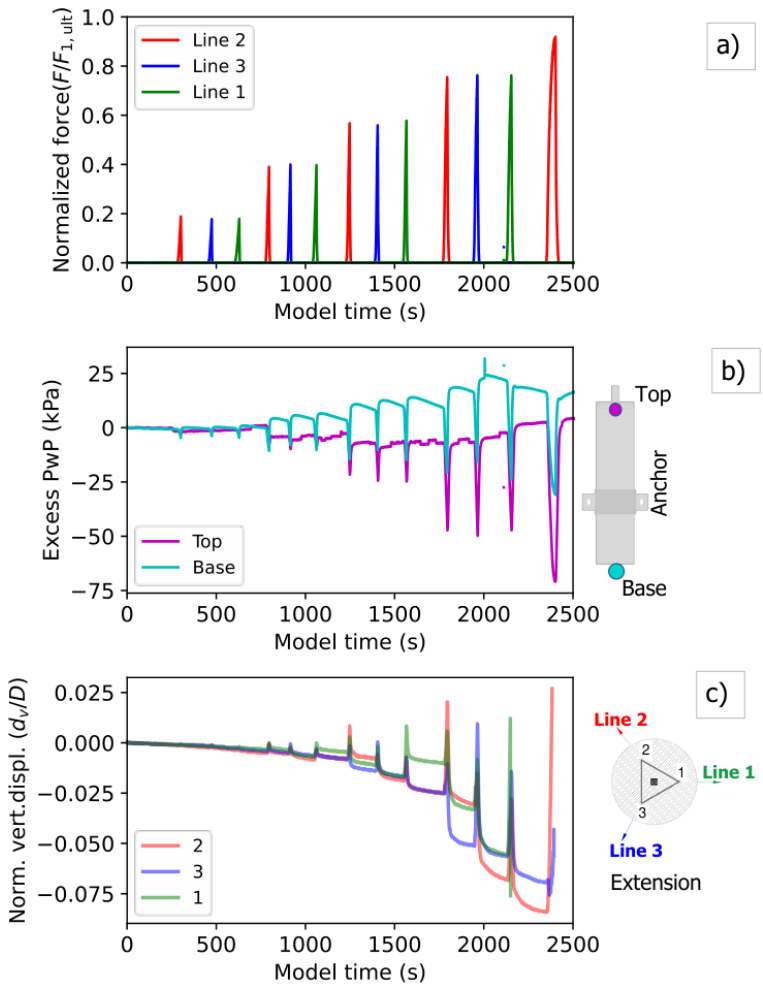

Figure 14. Anchor 2: alternated monotonic load with increasing magnitude, excess pore pressures and vertical displacements response

3.3 Multidirectional alternated load by two simultaneous mooring lines test – Anchor 3

Figure 15 shows the load–displacement curves for Anchor 3, where loads were applied simultaneously through two mooring lines. The results are presented in terms of the resultant force and displacement, as defined in Figure 9b. Although each mooring line was inclined at 45° to the horizontal, the combination of two inclined loads produced a resultant force with a higher average inclination of approximately 63°. Additionally, the normalized forces exceeded $F/F_{1,ult}$ = 1.0 when referenced to the baseline capacity of Anchor 1. The load–displacement curves for the different mooring line pairs exhibit similar trends in stiffness and shape, although they differ from the response observed for Anchor 1. This deviation is likely due to the steeper load inclination in the bidirectional configuration. After the bidirectional loading sequence, a final monotonic pull was

applied through Line 2. In this case, a reduced anchor capacity was observed, reaching a plateau at a load of 2.5 MN, corresponding to $F/F_{1,ul} \approx 0.63$.

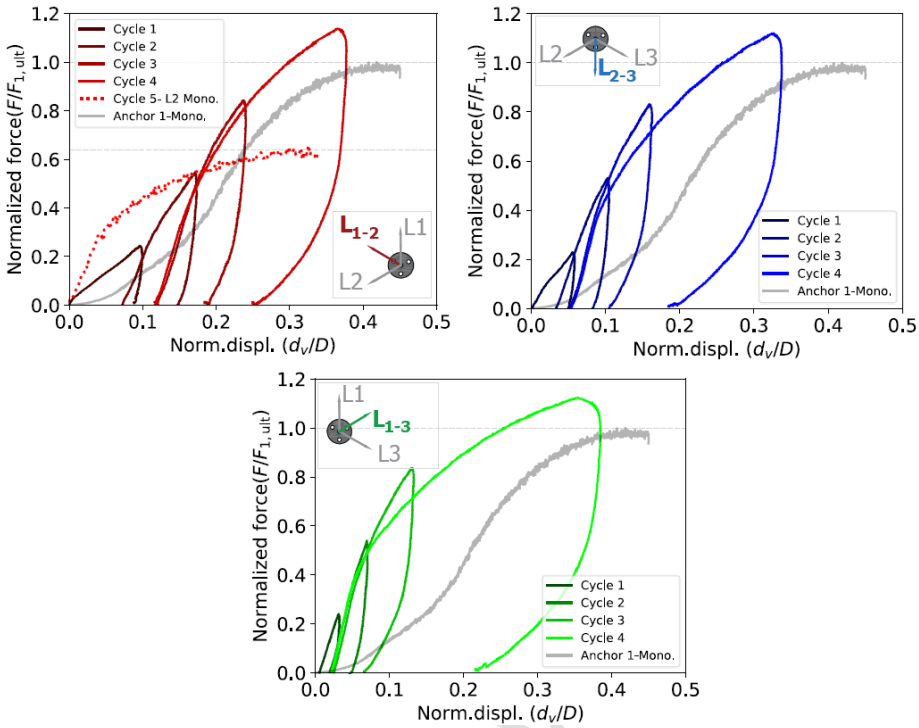

Figure 15. Anchor 3: Resultant force- displacement curves for simultaneous loads applied by two mooring lines simultaneously

Figure 16 summarizes the relationship between the resultant force components and the average vertical displacement of anchor 3. During the first three cycles, the anchor generally returned to its initial position after unloading, with relatively narrow load–unload loops indicating limited permanent deformation. In Cycle 4, however, larger upwards displacements were recorded, reaching approximately 0.4*D*. This cycle exhibited a clear upwards trend, resulting in permanent vertical displacement in the pullout direction.

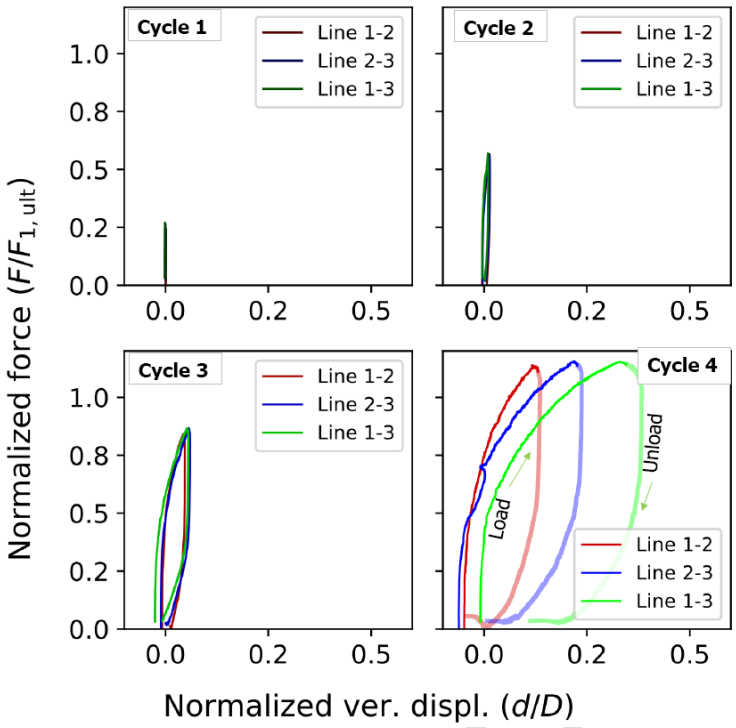

Figure 16. Anchor 2: Relationship between applied load and average vertical displacements

Figure 17a presents the resultant bidirectional forces applied during the test, showing consistent performance of the load control system across the defined load levels. The excess pore pressure responses measured at the anchor base and at a depth of one anchor diameter (1D) below the base are shown in Figure 17b and generally follow similar trends. Negative excess pore pressures developed during loading, with magnitudes proportional to the applied loads. An exception occurred during the final loading stage, which involved a monotonic pull applied to Line 2. In this case, the pore pressure response was less pronounced, suggesting that prior bidirectional loading caused accumulated uplift displacements (Figure 17c), reducing the anchor's ability to mobilize significant suction pressures.

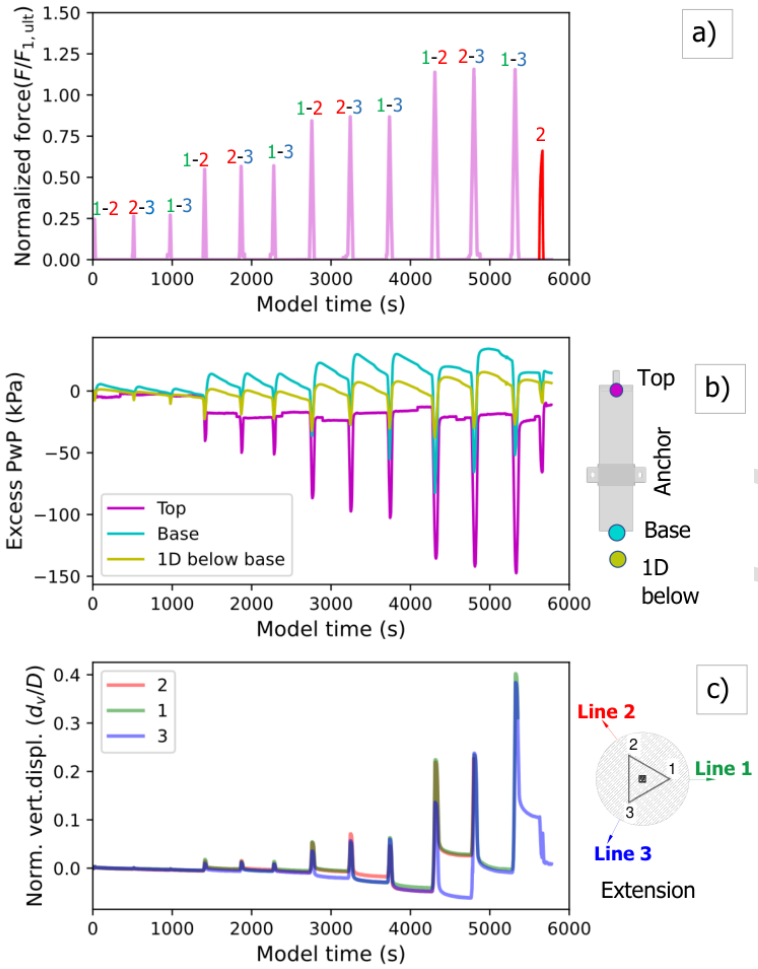

Figure 17. Anchor 3: alternated monotonic load by two simultaneous mooring lines with increasing magnitude, excess pore pressures and vertical displacements response

3.4 Digital image correlation analysis

Figure 18 presents the trajectory of the marker positioned at the top of the anchor extension in the x–y (horizontal) plane for Anchors 2 and 3, which was obtained using Digital Image Correlation (DIC) and linear laser displacement sensors. As the laser sensors were positioned below the marker location, a geometric scale factor was applied to approximate the marker displacements from the laser data. It is important to note that these measurements do not represent displacements at the anchor top or at the load application point but rather at the location of the marker used for DIC validation. This setup was implemented to enable a qualitative comparison between the responses of Anchors 2 and 3 and can be extended to more complex load paths or other foundation types, such as monopiles.

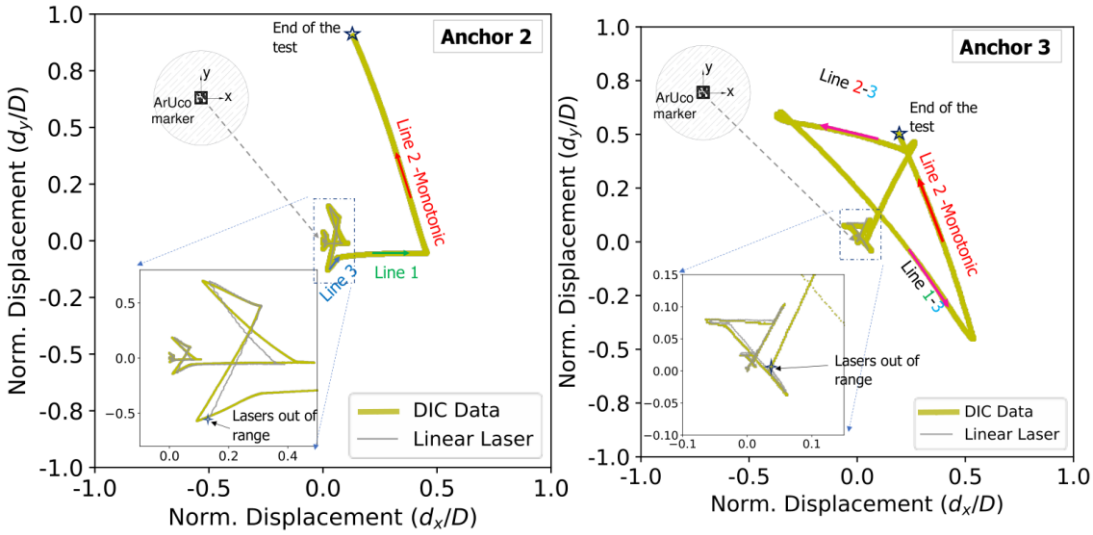

Figure 18. Trajectory of the ArUco marker, placed on the extension piece during anchor 2 and anchor 3 tests

Owing to the limited range of the laser sensors, the full displacement path could not be captured during the later stages of the test. Nevertheless, within their operational range, the laser and DIC measurements show good agreement. Compared with Anchor 2, Anchor 3, subjected to simultaneous bidirectional loading, exhibited a wider range of horizontal displacement. This increased response is attributed to the combined effect of two inclined loads acting concurrently, resulting in greater mobilization of the anchor. The most significant displacement increments were observed during the final three load–unload cycles and the subsequent monotonic pull.

Finally, DIC measurements are limited to a two-dimensional projection in the x–y plane. As a result, the recorded displacements may include both translational and rotational components, which cannot be fully separated using the current single-camera configuration.

3.5 Anchor capacity evaluation using experimental eesults and analytical envelope

A finite element simulation of the anchor capacity was conducted using BIFURC (NGI, 1997) to estimate the lateral and vertical load capacities when loading was applied at a depth corresponding to two-thirds of the anchor length. On the basis of the undrained shear strength profile obtained from the T-bar tests (Figure 11), the ultimate lateral capacity was estimated as H_{ult} = 3.1 MN and the vertical capacity was V_{ult} = 4.0 MN. The failure envelope shown in Figure 19 was constructed using the analytical formulation proposed by Supachawarote et al. (2004)

(Equation 1), which accounts for normally consolidated clay with increasing undrained strength with depth.

$$\left(\frac{H}{H_{ult}}\right)^{\frac{L}{D}+0.5} + \left(\frac{V}{V_{ult}}\right)^{\frac{L}{3D}+4.5} = 1 \quad (1)$$

where L is the length of the anchor and D, is the anchor's diameter.

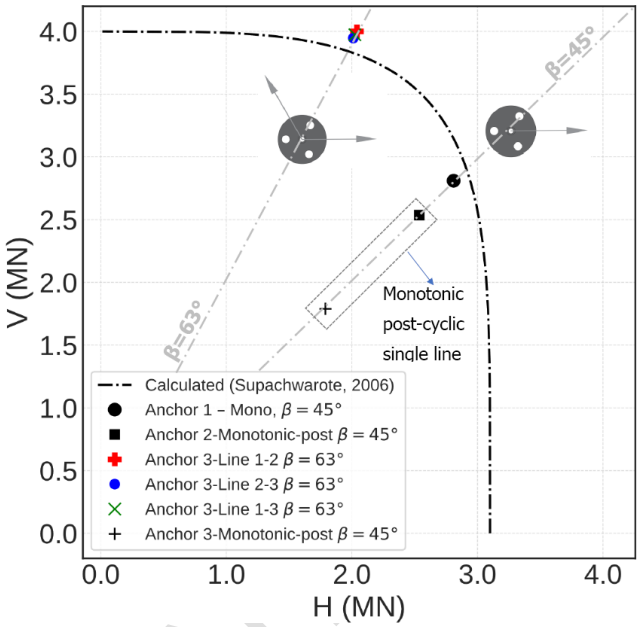

Figure 19. Horizontal–vertical (H–V) failure envelope with comparison to the load responses from Anchors 1 to 3

The results, presented in prototype scale units, show that the monotonic test on Anchor 1 (load inclination β = 45°) closely aligns with the estimated failure envelope. In contrast, the bidirectional load tests, with a combined load inclination of approximately β = 63°, produced data points slightly above the failure envelope during the final load cycle. The shape of the failure envelope and the experimental data points suggest that, for the tested configuration and anchor geometry, the vertical load capacity exceeds the lateral capacity. The post-cyclic monotonic tests, also with a 45° load inclination, revealed a reduction in anchor capacity, highlighting the influence of prior loading history on anchor performance.

Conclusions

This study presented a centrifuge testing programme aimed at investigating the behaviour of suction anchors in normally consolidated clay under simplified multidirectional loading scenarios. These tests served as a proof of concept for a newly developed experimental setup

designed to apply controlled inclined loads from multiple mooring lines, as a step toward more realistic simulations of shared anchor systems for floating offshore wind turbines (FOWTs). The main objective was to assess the functionality and performance of a newly developed experimental setup capable of applying controlled inclined loads from multiple mooring lines.

Key findings include:

The experimental setup successfully enabled the application of controlled multidirectional loading through an anchor design incorporating multiple padeyes. The load control system performed consistently according to predefined load sequences. The combined use of laser displacement sensors and DIC demonstrates the potential to monitor more complex load paths, including realistic time histories and cyclic loading, confirming the setup's suitability for advanced testing campaigns.

The monotonic inclined load test on Anchor 1 established a baseline ultimate capacity of approximately 4 MN, serving as a reference for evaluating subsequent multi-directional load responses.

Anchor 2, subjected to alternating loads from three mooring lines, showed progressive accumulation of downward displacement. The final monotonic pull demonstrated a capacity reduction of approximately 10% compared to the baseline, suggesting that load history and directionality influence anchor response.

Anchor 3, tested under simultaneous two-line loading, exhibited greater horizontal and upward displacements than Anchor 2. The increased load magnitude and steeper inclination angle (average 63°) led to a final monotonic capacity reduction of approximately 38% relative to Anchor 1, indicating a more pronounced degradation in holding capacity under the bidirectional load paths applied.

Negative excess pore pressures were consistently mobilised near both the anchor base and top, confirming 'suction resistance' (reverse end bearing) mobilisation. However, this effect progressively diminished with repeated bidirectional loading, likely due to accumulated uplift displacements compromising the anchor's sealing capacity and reducing its ability to generate suction pressures.

Digital image correlation (DIC) successfully tracked anchor displacements in the horizontal plane and showed good agreement with laser displacement measurements. The

analysis revealed more extensive horizontal displacement patterns of the anchor subjected to bidirectional loading. The current setup could be enhanced with multicamera systems to better capture three-dimensional anchor movement, including rotation.

Overall, this study provides a validated experimental setup and benchmark dataset for future investigations into suction anchor behaviour under complex loading paths. While the current experiments focused on simplified monotonic scenarios, the system is designed to support further testing under fully cyclic and time-dependent loading conditions. The results offer a foundation for the development and calibration of numerical models to support the design of shared anchoring systems for floating offshore wind.

Acknowledgements

This project has received funding from the European Union's Horizon 2020 research and innovation programme under the Marie Skłodowska-Curie grant agreement No. 101106921 – Shared Anchors for Floating Wind Turbines. The authors acknowledge Dr. Hans Peter Jostad and the Norwegian Geotechnical Institute (NGI) for providing access to the BIFURC software. The technical support of the centrifuge team at the Université Gustave Eiffel CG Lab during the preparation and execution of the tests is also acknowledged.

References

Cerfontaine B, White D, Kwa K, Gourvenec S, Knappett J and Brown M (2023) Anchor geotechnics for floating offshore wind: Current technologies and future innovations. Ocean Engineering 279: 114327, https://doi.org/10.1016/j.oceaneng.2023.114327

Chen W and Randolph MF (2007) Uplift capacity of suction caissons under sustained and cyclic loading in soft clay. Journal of Geotechnical and Geoenvironmental Engineering 133(11): 1352–1363.

Chen W and Randolph MF (2007) External radial stress changes and axial capacity for suction caissons in soft clay. Géotechnique 57(6): 499–511, https://doi.org/10.1680/geot.2007.57.6.499

Cheng X, Wang J and Wang Z (2016) Incremental elastoplastic FEM for simulating the deformation process of suction caissons subjected to cyclic loads in soft clays. Applied Ocean Research 59: 274–285, https://doi.org/10.1016/J.APOR.2016.05.015

Corte J (1984) The L.C.P.C. Centrifuge. In Proceedings of the Symposium on Recent Advances in Geotechnical Centrifuge Modeling. https://escholarship.org/uc/item/73k7s64v

Coughlan K, Davis M, Westgate Z, Lee J, Arwade S, Martin B and DeGroot D (2025) Design and analysis of shared anchor layouts for floating wind farms in deep waters. Ocean Engineering 320: 120208, https://doi.org/10.1016/j.oceaneng.2024.120208

Devin MC, DuPont BL, Hallowell ST and Arwade SR (2021) Optimizing the cost and reliability of shared anchors in an array of floating offshore wind turbines. ASME J. Risk Uncertainty Part B 7(4): 040905, https://doi.org/10.1115/1.4051163

Diaz BD, Rasulo M, Aubeny CP, Fontana CM, Arwade SR, DeGroot DJ and Landon M (2016) Multiline anchors for floating offshore wind towers. In OCEANS 2016 MTS/IEEE Monterey. IEEE, pp. 1–9, https://doi.org/10.1109/OCEANS.2016.7761374

Divall S, Taylor RN and Xu M (2016) Centrifuge modelling of tunnelling with forepoling. International Journal of Physical Modelling in Geotechnics 16(2): 83–95, https://doi.org/10.1680/jphmg.15.00019

Dyvik R, Andersen KH, Hansen SB and Christophersen HP (1993) Field tests of anchors in clay – I: Description. Journal of Geotechnical Engineering 119(10): 1515–1531, https://doi.org/10.1061/(ASCE)0733-9410(1993)119:10(1515)

Fontana CM, Hallowell ST, Arwade SR, DeGroot DJ, Landon ME, Aubeny CP, Diaz B, Myers AT and Ozmutlu S (2018) Multiline anchor force dynamics in floating offshore wind turbines. Wind Energy 21(11): 1177–1190, https://doi.org/10.1002/we.2222

Fu D, Lai Y, Xiong G and Zhu B (2024) Centrifuge modeling of the performance of suction anchor in soft clay. J. Offshore Mech. Arct. Eng. 146(5): 052102, https://doi.org/10.1115/1.4064617

Garnier J, Gaudin C, Springman SM, Culligan PJ, Goodings D, Konig D, Kutter B, Phillips R, Randolph MF and Thorel L (2007) Catalogue of scaling laws and similitude questions in geotechnical centrifuge modelling. International Journal of Physical Modelling in Geotechnics 7(3): 1–23, https://doi.org/10.1680/ijpmg.2007.070301

Garrido-Jurado S, Muñoz-Salinas R, Madrid-Cuevas FJ and Marín-Jiménez MJ (2014) Automatic generation and detection of highly reliable fiducial markers under occlusion. Pattern Recognition 47(6): 2280–2292, https://doi.org/10.1016/j.patcog.2014.01.005

Gourvenec S (2020) Whole-life geotechnical design: What is it? What's it for? So what? And what next? In Proceedings of the 4th International Symposium on Frontiers in Offshore Geotechnics. Deep Foundations Institute, pp. 206–246.

Goupee AJ, Koo BJ, Kimball RW, Lambrakos KF and Dagher HJ (2014) Experimental comparison of three floating wind turbine concepts. J. Offshore Mech. Arct. Eng. 136(2): 020906, https://doi.org/10.1115/1.4025804

Hirai H (2017) Assessment of cyclic response to suction caisson in clay using a three-dimensional displacement approach. Marine Georesources & Geotechnology 36(7): 805–817, https://doi.org/10.1080/1064119X.2017.1386743

James R and Ros MC (2015) Floating offshore wind: Market and technology review. The Carbon Trust, Report 439. See https://www.carbontrust.com/our-work-and-impact/guides-reports-and-tools/floating-offshore-wind-market-technology-review (accessed 22/05/2025)

Jiang Z (2025) Mooring design for floating wind turbines: A review. Renewable and Sustainable Energy Reviews 212: 115231, https://doi.org/10.1016/j.rser.2024.115231

Khemakhem M (2012) Etude expérimentale de la réponse aux charges latérales monotones et cycliques d'un pieu foré dans l'argile. Ph.D. thesis, Ecole Centrale de Nantes. URL: http://www.theses.fr/2012ECDN0026

Lau BH (2015) Cyclic behaviour of monopile foundations for offshore wind turbines in clay. Doctoral dissertation, University of Cambridge.

Lee J and Aubeny CP (2023) Effect of shared anchor system for a floating offshore wind project on reductions in CO_2 emissions. In Offshore Technology Conference, Houston, Texas, USA. https://doi.org/10.4043/32662-MS

Lee MJ, Gilo A, Park SJ and Choo YW (2024) Centrifuge model test on the bearing capacity of suction anchors subjected to monotonic and cyclic inclined pullout loads in clay. KSCE Journal of Civil Engineering: 100113, https://doi.org/10.1016/j.kscej.2024.100113

LIROS (2025) LIROS Rope Catalogue 2024/2025. Retrieved from: LIROS_rope_catalogue_2024_2025_eng_210_x_297_mm___low_res.pdf

NGI (1997) BIFURC-version 3, Undrained capacity analyses of clay. NGI Report 514052-1.

Ore Catapult and Arup (2024) Floating Offshore Wind Anchor Review. Public summary report PN000585-RPT-005 - Rev. 01. See https://fowcoe.co.uk/wp-

content/uploads/2024/03/FOWCoE-Report-Anchor-Review-PN000585-RPT-005-MA03.pdf (accessed 22/05/2025)

Panchal JP, McNamara AM and Goodey RJ (2020) Sheet pile groups as an alternative foundation solution to cast-in-situ concrete piles. International Journal of Physical Modelling in Geotechnics 20(2): 83–96, https://doi.org/10.1680/jphmg.18.00053

Pillai AC, Gordelier TJ, Thies PR, Dormenval C, Wray B, Parkinson R and Johanning L (2022) Anchor loads for shallow water mooring of a 15 MW floating wind turbine — Part I: Chain catenary moorings for single and shared anchor scenarios. Ocean Engineering 266(Part 1): 111816, https://doi.org/10.1016/j.oceaneng.2022.111816

Raines RD and Garnier J (2004) Physical modeling of suction piles in clay. In Proceedings of the ASME 2004 23rd International Conference on Offshore Mechanics and Arctic Engineering. ASME, Reston, VA, USA, pp. 621–631.

Sloan C, Hall M, Housner S, Lozon E and Sirnivas S (2022) Shared mooring systems for deep-water floating wind farms. Technical Report, NYSERDA Contract 142869. See https://nationaloffshorewind.org/wp-content/uploads/142869_Final-Report.pdf (accessed 22/05/2025)

Soriano C, Almeida MCF, Madabhushi SPG, Stanier S, Almeida MSS, Liu H and Borges RG (2022) Seismic centrifuge modeling of a gentle slope of layered clay, including a weak layer. Geotechnical Testing Journal 45(1): 125–144, https://doi.org/10.1520/GTJ20200236

Springman SM (1993) Centrifuge modelling in clay: Marine applications. Technical Rep. No. CUED/D-SOILS/TR260, University of Cambridge, Cambridge, UK. See https://www-geo.eng.cam.ac.uk/system/files/documents/tr-260-centrifuge-modelling-in-clay-marine.pdf (accessed 22/05/2025)

Stewart DP and Randolph MF (1991) A new site investigation tool for the centrifuge. In Proceedings of the International Conference on Centrifuge Modelling, Centrifuge '91, Boulder, CO, 13–14 June 1991. Balkema, Rotterdam, the Netherlands, pp. 531–538.

Supachawarote C, Randolph MF and Gourvenec S (2004) Inclined pull-out capacity of suction caissons. In Proceedings of the Fourteenth International Offshore and Polar Engineering Conference, Toulon, France, May 2004.

Thorel L, Ferber V, Caicedo B and Khokhar IM (2011) Physical modelling of the wetting-induced collapse of an embankment base. Géotechnique 61(5): 409–420, https://doi.org/10.1680/geot.10.P.029

Vlasblom M (2018) The manufacture, properties, and applications of high-strength, high-modulus polyethylene fibers. In Bunsell AR (Ed.), Handbook of Properties of Textile and Technical Fibres (2nd ed., pp. 699–755). Woodhead Publishing, https://doi.org/10.1016/B978-0-08-101272-7.00018-3

Xu H, Rui S, Shen K, Jiang L, Zhang H and Teng L (2024) Shared mooring systems for offshore floating wind farms: A review. Energy Reviews 3(1): 100063, https://doi.org/10.1016/j.enrev.2023.100063

Zhou M, Yang N, Tian Y and Zhang X (2023) Inclined pullout capacity of suction anchors in clay over silty sand. Journal of Geotechnical and Geoenvironmental Engineering 149(6): 04023030.

Figure Captions

Figure 1. Target pre-consolidation pressures to build a normally consolidated clay profile (right axis in prototype scale)

Figure 2. Plan view of the experimental setup: location of the suction anchors

Figure 3. Experimental setup for multiline anchor testing. a) Perspective view of the model container and actuators. b) Detailed view of an anchor and instrumentation.

Figure 4. Rotating assembly to test various anchor locations

Figure 5. a) Detail of a model anchor; b) guide mechanism for installation; c) anchor installation at 1-g

Figure 6. A view of a model anchor and instrumentation after installation at 1-g

Figure 7. Model instrumentation. a) Lateral view or an anchor and connection of one mooring line. b) Linear lasers position to track lateral displacements. c) Point lasers to track vertical displacements and detail of an ArUco marker

Figure 8. Anchor 2: progressively increasing amplitude monotonic loads applied by alternating mooring lines

Figure 9. Anchor 3: progressively increasing amplitude monotonic loads applied by two mooring lines simultaneously.

Figure 10. Undrained shear strength profiles measured in-flight and 1-g shear hand vane tests

Figure 11. Anchor 1: load-displacement response and excess pore pressure measurements at the top and at the base of the anchor

Table Captions